2012

Ferromagnetism in Li doped ZnO nanoparticles: The role of interstitial Li

Saif Ullah Awan
Quaid-i-Azam University, Virginia Commonwealth University

S. K. Hasanain
Quaid-i-Azam University

Massimo F. Bertino
Virginia Commonwealth University, mfbertino@vcu.edu

G. Hassnain Jaffari
Virginia Commonwealth University

Awan, S. U., Hasanain, S. K., & Bertino, M. F., et al. Ferromagnetism in Li doped ZnO nanoparticles: The role of interstitial Li. Journal of Applied Physics, 112, 103924 (2012).

Ferromagnetism in Li doped ZnO nanoparticles: The role of interstitial Li

Saif Ullah Awan,[1,2,a)] S. K. Hasanain,[1] Massimo F. Bertino,[2,3] and G. Hassnain Jaffari[1]
[1]*Department of Physics, Quaid-i-Azam University, Islamabad 45320, Pakistan*
[2]*Department of Physics, Virginia Commonwealth University, Richmond, Virginia 23284, USA*
[3]*Nanomaterials Core Characterization, Virginia Commonwealth University, Richmond, Virginia 23284, USA*

(Received 23 September 2012; accepted 26 October 2012; published online 30 November 2012)

ZnO nanoparticles doped with Li ($Zn_{1-y}Li_yO$, $y \leq 0.1$) have been investigated with emphasis on the correlation between their magnetic, electronic, and structural properties. In particular, defects such as interstitial Li and Zn atoms, substitutional Li atoms, and oxygen vacancies have been identified by X-ray photoelectron spectroscopy (XPS) and their respective roles in stabilization of the magnetic moment are discussed. X-ray diffraction (XRD) and XPS give clear evidence of Li presence at both substitutional and interstitial sites. XPS studies further show that the amount of substitutional Li defects (Li_{zn}) and interstitial Li defects (Li_i) vary non-monotonically with the Li concentration, with the Li_i defects being noticeably high for the $y = 0.02$, 0.08, and 0.10 concentrations, in agreement with the XRD results. Magnetization studies show room temperature ferromagnetism in these nanoparticles with the moment being largest for the particles with high concentration of interstitial lithium and vice versa. Both interstitial Zn (Zn_i) defects and Zn-O bonds were determined from the Zn LMM Auger peaks; however, the variation of these with Li concentrations was not large. Oxygen vacancies (V_o) concentrations are estimated to be relatively constant over the entire Li concentration range. We relate the Li_i and Zn_i defects to the formation and stabilization of Zn vacancies and thus stabilizing the p-type ferromagnetism predicted for cation (zinc) vacancy in the ZnO type oxides. © *2012 American Institute of Physics*.
[http://dx.doi.org/10.1063/1.4767364]

I. INTRODUCTION

Ideal materials for spintronics applications should be a dilute magnetic semiconductor (DMS) without any transition metal atoms, independently controllable carrier density, and carrier density dependent magnetization with high Curie temperature.[1,2] Ferromagnetism (FM) in *p*-type ZnO systems without transition metal dopents is preferable for spintronics applications.[3] Undoped ZnO usually exhibits *n*-type behavior due to the presence of Zn interstitial (Zn_i) and oxygen vacancies (V_o) defects. In last many decades, the bottleneck in the development of p-type ZnO based materials and devices for practical applications has proven to be the low solubility limit of acceptor dopents, formation of deep acceptor levels and self-compensating effects.[4] *P-type* conductivity in ZnO requires the incorporation of shallow acceptor levels which may be possible by substituting monovalent atoms at Zn sites that creates one hole per substituent at the neighboring oxygen atom.[5] Ferromagnetism due to these holes, sometimes involving defect complexes, has been predicted on the basis of local density functional and other calculations. Peng *et al.*[6] pointed out that a threshold hole concentration is necessary to induce room temperature ferromagnetism (RTFM). Therefore, to induce ferromagnetic behavior in ZnO, one way is to stabilize cation (Zn) vacancies and produce holes at the same time. This can be made possible by doping with suitable elements, in particular, using Lithium (Li), which while being a hole dopant (monovalent) can also be easily incorporated into ZnO, and it is often used to produce p-type ZnO materials.[7,8]

Doping of Li in ZnO has been studied theoretically by several groups[7–10] using different methods. Lander[9] reported that Li may behave both as an acceptor and as a donor in ZnO. The acceptor behavior is exhibited when Li substitutes at a Zn site (Li_{Zn}) and the donor behavior arises when Li occurs at an interstitial site (Li_i). Defects such as Li_{Zn} are theoretically predicted to have a shallow acceptor level in ZnO.[10] Park *et al.*[10] who measured the ionization energy of 90 meV for Li_{Zn} defects have argued that the p-type doping efficiency of Li is limited due to the formation of compensating interstitial defects. Calculations performed by Wardle *et al.*[11] indicated that the neutral Li_{Zn}–Li_i complex is relatively stable with a dissociation energy of 1.5 eV. The dissociation of the Li_{Zn}–Li_i pair into Li_{Zn} and diffusion of Li_i is expected to occur at 300 °C. Wardle *et al.*[11] suggested that *p*-type doping may be limited by the formation of some other complexes such as Li_{Zn}–H and Li_{Zn}–Li_i complex. Lee and Chang[12] proposed that H can help to enhance the solubility of Li and that subsequent H removal can potentially result in low-resistivity *p*-type ZnO. The co-doping of Li with H, in the form of hydrogen–acceptor complexes, is suggested as an effective way of increasing the concentration of Li_{Zn} acceptors. The activation of the hydrogen-passivated acceptor defects, they suggest, would be possible by post-growth annealing.[12] Li-doped p-type ZnO thin films were reported by Zeng *et al.*[13] with an activation energy of 150 meV for Li_{Zn}. They also reported a deeper acceptor level at 250 meV, which was assigned as Li related complexes.[13]

a)Author to whom correspondence should be addressed. Electronic mail: ullahphy@gmail.com.

A variety of magnetic studies have been performed on Li doped ZnO both in bulk and thin films form. Experimentally, some groups[14] have reported that Li doped ZnO nano materials are paramagnetic whereas some other groups[5,13,14] have seen FM behavior. Lin *et al.*[14] found paramagnetic behavior in spin coated polycrystalline Li doped ZnO thin films on Si substrate. In 2009, Chawla *et al.*[1] demonstrated that *p*-type Li doped ZnO nanocrystalline powder and pellets can exhibit high temperature FM up to 554 K. They propose that substitutional Li dopant induces moments on neighboring oxygen atoms which when considered in a correlated model for oxygen orbitals with random potentials may explain the observed FM and high Curie temperature. Chawla *et al.*[5] have also reported ferromagnetism in 2% Li-doped ZnO nanorods with Curie temperature up to 554 K. They observe p-type conductivity with the formation of shallow Li acceptor states at substitutional Zn sites. They also determined that magnetization and Curie temperature decrease with the enhancement of hole concentration. In 2010, Yi *et al.*[15] studied experimentally and theoretically p-type ferromagnetic Li doped ZnO thin film and found that complex defects ($V_{Zn} + Li_i + Li_{Zn}$) are responsible for controlling and tuning the ferromagnetism. They suggest that cation Zinc vacancies (V_{Zn}) are the origin of ferromagnetism in oxides base DMS. They demonstrated that the presence of nonmagnetic Li generates holes minimizes the formation energy of V_{Zn} and also stabilizes the V_{Zn} in ZnO thin films. In the light of these various, sometimes conflicting, reports the origin of ferromagnetism in ZnO due to doping of small concentrations of non-magnetic dopant (Li) and the understanding of this phenomenon is still a challenge.[15]

From the point of view of applications, ferromagnetic Li doped ZnO has the obvious advantage of eliminating the possibility of clustering of magnetic impurities which is a serious drawback for magnetic dopants, e.g., Co. Additionally, the optical properties of ZnO that emits UV and visible luminescence, coupled with the ferroelectric behavior reported in Li doped ZnO make it a very promising multifunctional material with a wide range of potential applications. To this end, we need to better understand the role of various defects that seem to strongly affect or even control the ferromagnetism in this system.

In this work, we have synthesized Li doped ZnO nanoparticles and have observed room temperature ferromagnetism. To the best of our knowledge, this is the first report of ferromagnetism in Li doped ZnO nanoparticles. Structural, electronic, and magnetic studies have been carried out on a range of Li concentrations and the variation of ferromagnetic properties has been correlated with the development of specific defects such as Li interstitials and the lack of dependence on some others such as O vacancies. Correspondence of our results with specific models of ferromagnetism in p-type ZnO has been discussed.

II. EXPERIMENTAL DETAILS

Zinc acetate dehydrate $Zn(CH_3COO)_2 \cdot 2H_2O$, and lithium acetate dehydrate $Li(CH_3COO) \cdot 2H_2O$ of Sigma-Aldrich (99.99% pure) commercial chemicals were used as starting precursors. Li doped ZnO [$Zn_{1-y}Li_yO$ ($y = 00$, 0.02, 0.04, 0.06, 0.08, and 0.10)] series of samples were synthesized by a low temperature chemical sol-gel technique.[16] The measured amount of solute (wt. %) was dissolved in 200 ml ethylene glycol ($C_2H_6O_2$) to form 0.1M solution. The suspension was stirred for about 30 min in conical flask and then heated with stirring at 180 °C for 180 min in oil bath with water cooling system. After the formation of precipitation of the precursors, the mixture was cooled down to room temperature. The solid wet phase was recovered by washing and centrifuging two times with ethanol and distilled water to separate the residues. Finally, we dried this wet solid in an oven at 100 °C overnight. In order to investigate the effect and role of oxygen vacancies with other defects (i.e., V_{zn}, Zn_i, Li_i and Li_{zn}), all samples were annealed in forming gas [$5\%H_2 + 95\%Ar$] at 600 °C.

The structural characterizations were performed by PANalytical X'perPRO X-ray diffractometer (XRD) using Cu K_α radiation $\lambda = 1.5405$ Å. X-ray photoelectron spectroscopy (XPS) was performed on a Thermo Scientific ESCALAB 250 spectrometer with a focused monochromatic Al K_α ($h\nu = 1486.6$ eV) source. A hemispherical analyzer with a 6-channeltron multichannel detector was used. The incident X-ray beam was 45° off normal to the sample while the X-ray photoelectron detector was normal to the sample to produce high signal-to-noise ratio. Since the sample may have non conductive layer, charge compensation was employed during the data collection using the internal flood gun (2 eV electrons) and a low energy Ar^+ external flood gun. To produce sufficient charge compensation, Ar gas pressure was kept at 1×10^{-8} mbar. The incident X-ray beam was focused onto 0.5×1 mm^2 spot at the sample. Constant analyzer energy (CAE) mode was utilized, and pass energy was set to 20 eV. A Quantum Designed Versa lab's vibrating sample magnetometer (VSM) was used to investigate the magnetic properties. The temperature range of VSM is 50–300 K and its maximum field strength is −3 T to +3 T.

A. Structural characterization

Crystal structure and phase analysis were performed using XRD. The as synthesized samples were amorphous (data not present here). Fig. 1(a) shows the polycrystalline XRD patterns for a series of $Zn_{1-y}Li_yO$ ($y = 00$, 0.02, 0.04, 0.06, 0.08, and 0.10) samples after annealing at 600 °C. A step size of 0.02 and time-per-step of 1.50 s were used for each scan. It is evident that only the peaks corresponding to the hexagonal ZnO wurtzite (SG $P63\ mc$, $a = 0.32$ nm, $c = 0.52$ nm JCPDS file No. 36-1451) structure were observed. XRD patterns of all the samples showed that they exhibit single phase with broad peaks characteristic of nanocrystalline size. To further confirm the complete absence of Lithium segregation, high resolution scans near the expected positions of Li_2O peaks were performed and no such phase was observed. The average crystallite size was calculated from the XRD data using the Debye Scherrer formula. The undoped ZnO sample had an average crystallite size of 65 nm, whereas the Li doped ZnO samples were about 22–48 nm in size.

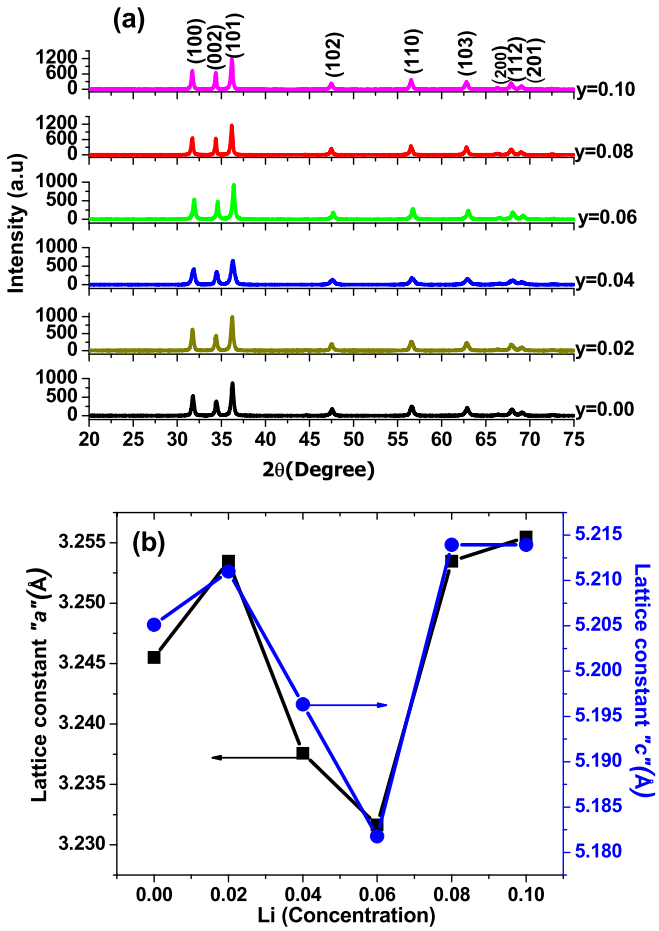

FIG. 1. (a) X-ray diffraction patterns of $Zn_{1-y}Li_yO$ (y = 0.00, 0.02, 0.04, 0.06, 0.08, and 0.10) nanoparticles. (b) Lattice parameters "*a*" and "*c*" of the $Zn_{1-y}Li_yO$ nanoparticles as a function of Li concentration (y).

XRD data exhibit small peak shift which ensured the homogeneous doping of Li in ZnO structure with no presence of clusters. From the XRD data, we obtained cell parameters "*a*" and "*c*" for the hexagonal wurtzite structure of ZnO as a function of increasing Li concentrations. The evolution of the hexagonal cell parameters of samples are shown in Fig. 1(b). We note that a decrease in the lattice parameters would, in general, be expected when Zn^{2+} ions are replaced by Li^{1+} ions, because of the smaller radius of Li ions (0.060 nm) as compared to the Zn^{2+} ions (0.074 nm) while the lattice parameters will tend to increase when Li ions incorporate at interstitial sites.[15] The expansion of lattice parameters for Li at. % 2, 8, and 10 samples as compared to pure ZnO sample, suggests that Li is incorporating in interstitial sites (Li_i) more as compared substitutional sites (Li_{zn}). In contrast, we found a decreasing trend of lattice parameters for the 4 and 6 at. % Li samples which suggests that in these intermediate compositions Li preferentially substitutes at the Zn sites (Li_{zn}) rather than occupying the interstitial sites (Li_i). The XPS results (to be discussed later) point towards a similar conclusion.

The non-monotonic trend of variation of the lattice parameter suggests that Li_i defects are more predominant generated at 2%, 8%, and 10% Li concentrations, while Li_{zn} defects are dominant at 4% and 6% Li doped samples. It has been noted in the literature[15] that Li atoms prefer interstitial sites at low concentration in thin films, while additional Li atoms replace Zn atoms when the Li doping concentration exceeds a certain threshold (3–4 at. %).

B. Electronic structure

To examine the extended role of the defects, e.g., as complexes that affect the ferromagnetic behavior we have carefully considered the electronic state of each of the atomic species and attempted to correlate the interstitial and substitutional role of Li atoms, simultaneously with the presence of oxygen vacancy defects. XPS has been used for this purpose. Binding energies of photoelectrons are standardized with the aliphatic hydrocarbon C 1s peak at 285 eV. All XPS spectra were deconvoluted using XPSPEAK41 software for Lorentzian-Gaussian fitting of asymmetric peaks by subtracting the Shirley background. No impurities were detected during measuring the XPS survey spectra (data not shown here) of all samples. The absence of any magnetic element to the extent of the XPS resolution indicates that any observed ferromagnetism would be intrinsic in nature.

To study the influence of Li doping in the ZnO samples, the high resolution XPS spectra of Zn, Li, and O were recorded. Fig. 2 shows the electron binding energy of Zn 2p core XPS spectra of 0%, 6%, and 10% Li doped samples. The binding energies of Zn 2p3/2 and 2p1/2 peaks are located around 1022.30 eV and 1045.40 eV, respectively, with spin-orbit splitting of 23.1 eV for undoped ZnO. We measured the Zn $2p_{3/2}$ and $2p_{1/2}$ spectra peaked at 1022.35 ± 0.02 and 1045.45 ± 0.02 eV, respectively, for all samples. From the observed spin-orbit splitting ($\Delta_{Zn} = 23.1$ eV) and the binding energy positions of the two strong peaks of core level Zn 2p XPS spectra and from their line width, it has been concluded that Zn atoms are in Zn^{2+} oxidation state.[17] However, the measured binding energy values of Zn 2p for Zn-O bonding are on the higher binding energy side compared to metallic Zn for which the core level Zn 2p3/2 binding energy position is 1021.50 eV.[17] The Zn 2p3/2 and 2p1/2 spectra exhibit

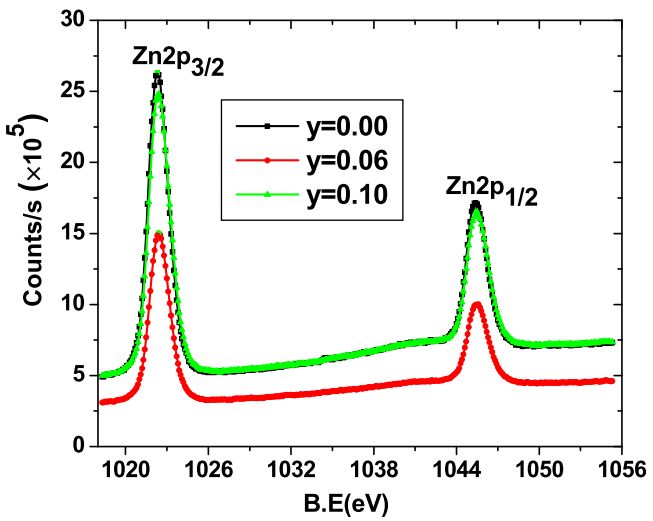

FIG. 2. XPS of Zn ($2p_{3/2}$ and $2p_{1/2}$) core level spectra of $Zn_{1-y}Li_yO$ (y = 0.00, 0.06, and 0.10) nanoparticles recorded at room temperature.

symmetric features which rule out the possibility of multi component of Zn.

Auger peaks of Zn were obtained from the XPS survey spectra to measure the presence of interstitial Zn (Zn_i) defects. Auger peaks show larger shape changes than XPS spectra to identify the different chemical sates of atoms, because mostly three electrons are involved with many body effects in a single Auger transition, as reported.[18] We observed that high resolution XPS spectra of Zn 2p peaks had symmetric feature whereas Auger peaks usually showed asymmetric shape. Hence, for determining the chemical state of Zn atoms, the analysis of Zn LMM Auger peaks has been utilized to quantify Zn interstitials versus Zn-O. Typical measured Auger peak Zn $L_3M_{4,5}M_{4,5}$ of 6% Li doped ZnO sample was deconvoluted. The two Lorentzian-Gaussian fitted Auger peaks of 6% Li doped ZnO sample that are attributed to the Zn-O bond and Zn_i which are located centrally at higher binding energy 497.6 eV and lower binding energy 493.95 eV, respectively,[18] are plotted in Fig. 3(a). The relative area obtained from the peaks deconvolution for the entire series, was utilized to extract Zn_i defects concentration Zn-O bond and are shown in the Fig. 3(b) for all compositions. In ZnO samples annealed at higher temperatures, Zn interstitials are usually found to be located between O^{2-} and Zn^{2+} positions[18] accompanied by Zn vacancies (V_{zn}). These V_{zn} defects may be responsible for ferromagnetic behavior in ZnO systems as has been reported.[19] In our samples, we find that with the increasing of Li concentration the concentration of Zn_i initially decreased up to 6% Li, while on further doping it increased up to 10% Li doped ZnO samples as shown in Fig. 3(b). It is understood that the generation of each Zn_i defect would, in general, be accompanied by the generation of a Zn vacancy. Qualitatively, the variations in both the Zn_i defects and lattice parameters (discussed above in the context of the XRD results), follow the same trend with increasing Li concentration in Li doped samples.

The XPS core level spectra of O-1s were measured and investigated as to how the oxygen concentration is varied upon Ar/H_2 annealing and whether or not it can be correlated with the observed ferromagnetic behavior (discussed later). At first glance, the spectrum is asymmetric indicating the possibility that multi-component of oxygen species was present. The typical asymmetric O-1s peaks can be fitted by three peaks as plotted in Fig. 4(a) for 2% Li doped. The relative

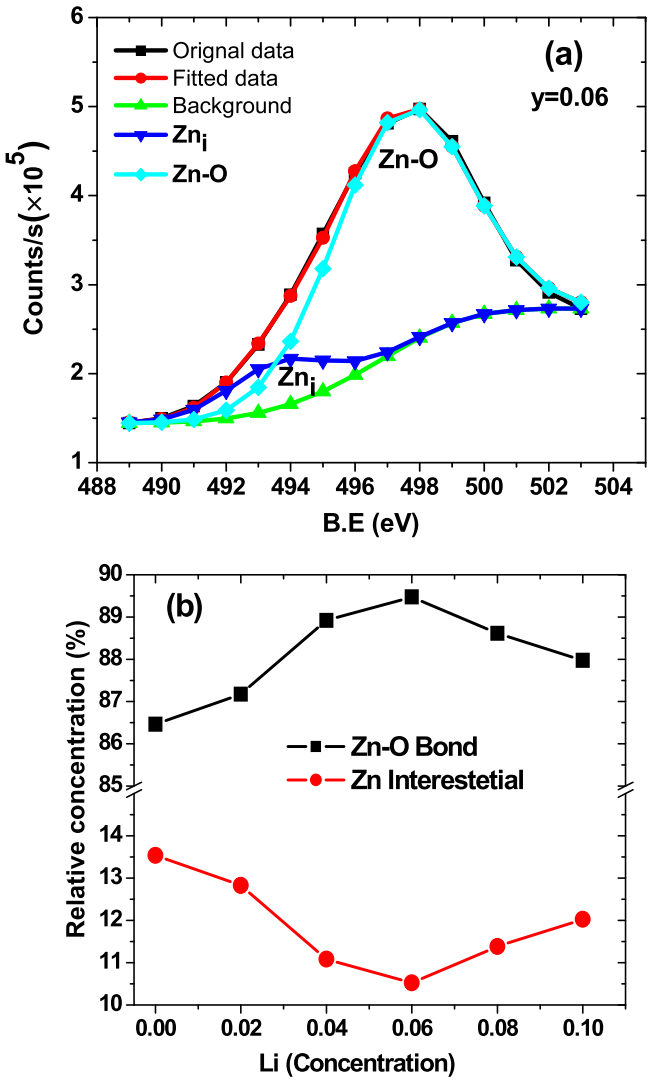

FIG. 3. (a) The original and deconvoluted Zn $L_3M_{4,5}M_{4,5}$ Auger peaks of y = 0.06 sample. (b) Variation in interstitial Zn (Zn_i) and Zn bonded with oxygen atoms (Zn-O) as a function of Li concentration.

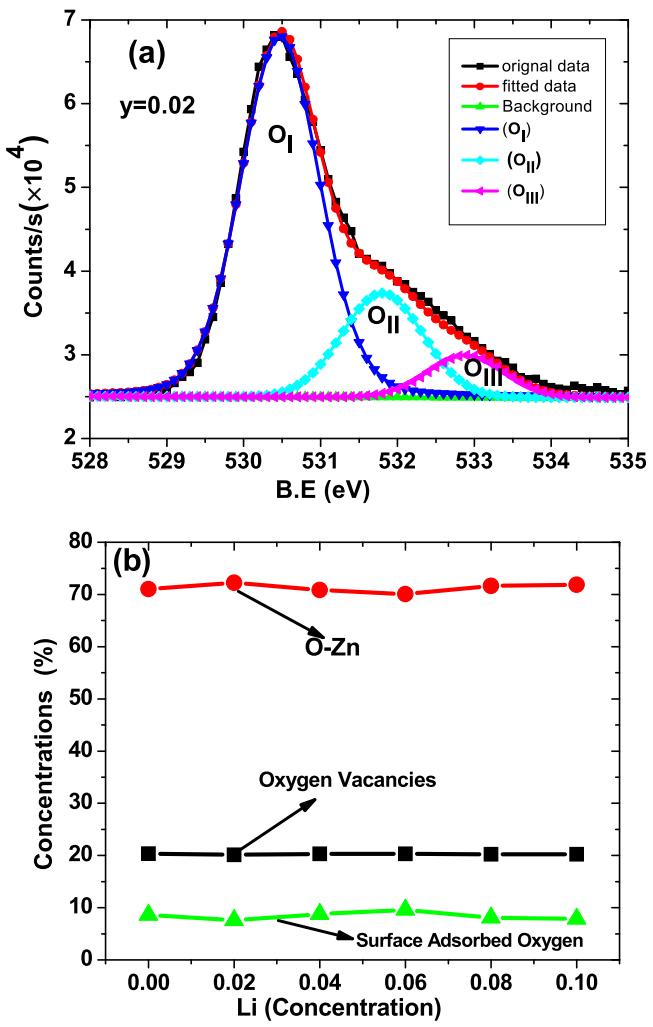

FIG. 4. (a) Deconvoluted O 1s XPS core level spectra of y = 0.02 sample. (b) The ratio of areas under the deconvoluted peaks, i.e., O_I, O_{II}, and O_{III} as a function of Li concentration (symbols are defined in text).

area of these deconvoluted peaks with a centered lower binding energy O_I (530.60 ± 0.02 eV), medium binding energy O_{II} (531.90 ± 0.02 eV), and high binding energy O_{III} (532.98 ± 0.02 eV) are shown in Fig. 4(b) for all samples. The fitted peaks indicate that each resolved component has a full width half maximum (FWHM) around 1.70 ± 0.2 eV, while the initial asymmetric O-1 s spectra have FWHM around 2.95 ± 0.2 eV.

The component O_I on the lower binding energy side of O-1s spectra is associated with Zn-O.[17,20] In other words, the area of this component is proportional to the amount of oxygen atoms in a fully oxidized stoichiometric surrounding the Zn atoms in tetrahedral symmetry. The medium binding energy component O_{II} centered at 531.90 ± 0.02 eV is typically associated with the oxygen vacancies (V_o), i.e., oxygen deficient regions in ZnO.[17,20] It was also noticed that the area of O_{II} component is lower than that of the O_I component. Therefore, in our samples, the changes in the area under the curve of this component may be connected to the variations in the concentration of V_o. We noticed and observed, however, that there is no significant variation in the area corresponding to V_o with variation of the Li concentration. Finally, we note that the high binding energy component O_{III} is due to the presence of chemisorbed surface hydroxyl, $-CO_3$, absorbed H_2O, or absorbed O_2.[17,20] The relevant areas of these deconvoluted peaks O_I, O_{II}, and O_{III} are plotted in Fig. 4(b) to illustrate the relative contribution of each component.

High resolution XPS scans were performed and analyzed for the identification of chemical bonding of Li atoms in all samples. The two Lorentzian-Gaussian fitted curves reveal that the Li-1s spectrum was asymmetric as plotted in Figs. 5(a)–5(c) for the $y = 0.02$, 0.06, and 0.10 compositions. The areas under these deconvoluted curves indicate the relative concentrations of Li at interstitial (Li_i) and substitutional (Li_{zn}) sites. The higher binding energy peak center at 55.70 eV is related to Li_{zn} and indicates the Li_{zn}-O bonds, while the lower binding energy curve centered at 52.9 eV can be assigned to the Li_i defects.[8,17] We note that for $y = 0.02$, 0.08, and 0.10, the relative intensity (integrated area) of low binding energy peak is high as compared to that for the higher binding energy peaks. In contrast for $y = 0.04$ and 0.06, the intensities of the respective high binding energy peaks (Li_{Zn}) are greater than those of low binding

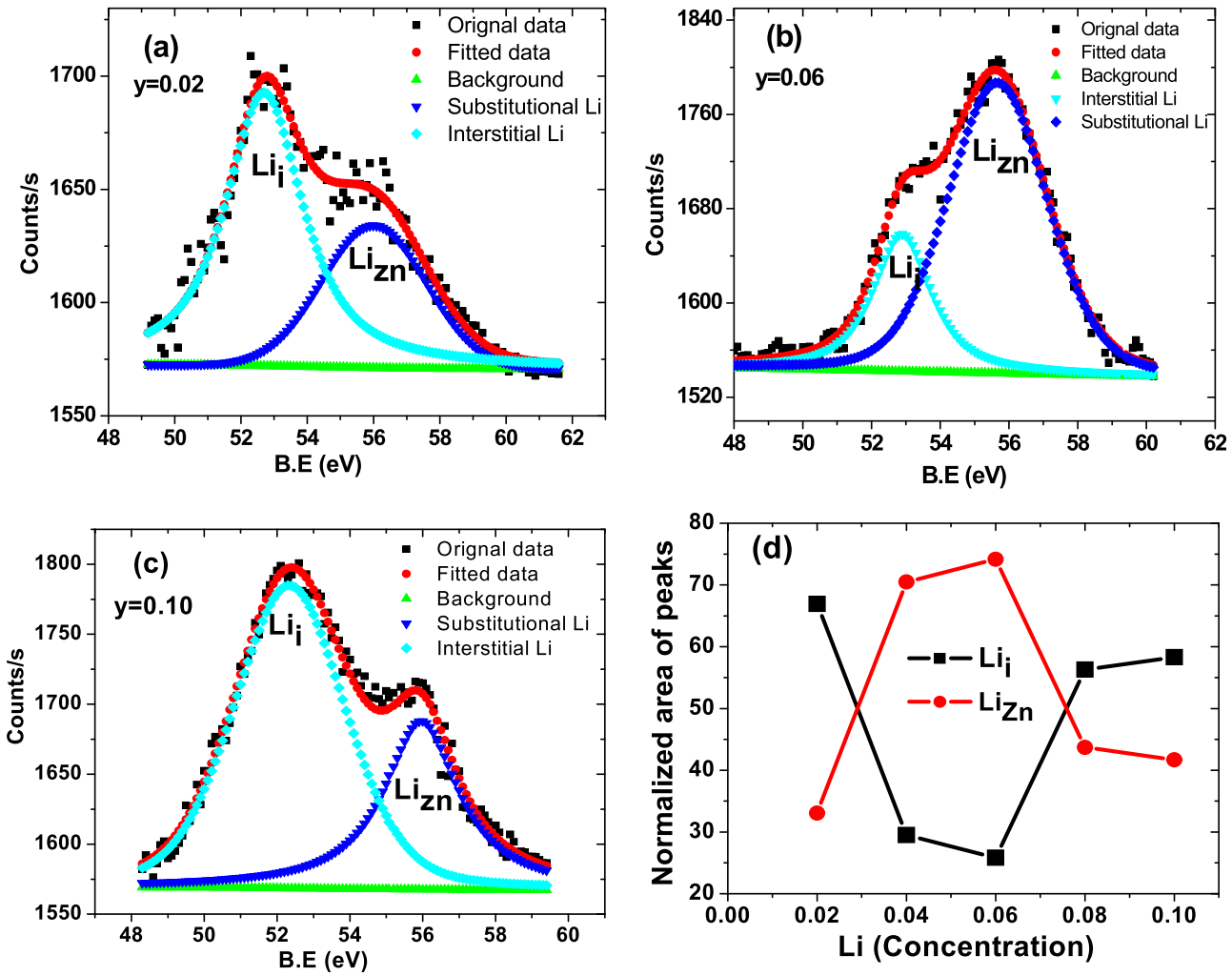

FIG. 5. XPS spectra of Li 1s core level for various concentrations, i.e., (a) $y = 0.02$, (b) $y = 0.06$, and (c) $y = 0.10$. (d) Normalized area under the deconvoluted peaks of interstitial and substitutional Li as a function of Li concentration.

energy peaks (Li_i). The variations in concentrations of these Li_{zn} and Li_i defects were estimated by plotting the area under the higher binding and lower binding energy curves as shown in Fig. 5(d) for doped sample and indicate that the 2%, 8%, and 10% concentrations have a higher percentage of interstitial Li. Within the limits of our technique, it appears that for the 2%, 8%, and 10% concentrations the Li_i defects constitute more than 50% of the total Li, while in the 4% and 6% they are less than 50%. We further note the clear correlation between the lattice parameters for the various compositions determined by the XRD and the Li_i defects estimated here. This trend is shown in Fig. 6. The large Li_i concentrations are accompanied by an expansion of the lattice parameter as may be expected. Finally, we note that since the Li is supposed to substitute at a zinc site, ideally, the presence of interstitial Lithium is itself an indicator of a vacant cation site (zinc vacancy). Hence, we suggest that the Li concentrations where the XPS indicates higher Li interstitials may also be read as systems with higher Zn vacancy concentrations. It is interesting to note that zinc vacancy while being a more energetic and hence unfavorable defect sitting alone, becomes more favorable in the neighborhood of a Li interstitial.[15] This is, we understand, the primary role that Li plays in this system, i.e., making Zn vacancies more favorable.

Summarizing the comparison of the trends seen in the XPS and XRD data, we note the following features. Interstitial Zn defects variations with Li concentration were not large. Similarly, oxygen vacancy concentration is estimated to be relatively constant over the entire Li concentration range. The variations in the lattice parameters and the estimated concentration of Li_{zn} defects display opposite trends with increasing Li concentration. These observations are important to highlight since variations in the trends of defects (V_{zn}, Li_i, and Li_{zn}) with varying Li concentration can play a significant role in determining the defect mediated ferromagnetism in such systems. In Sec. II C, we will emphasize how the variational trends of these defects play a vital role in tuning the ferromagnetism in samples.

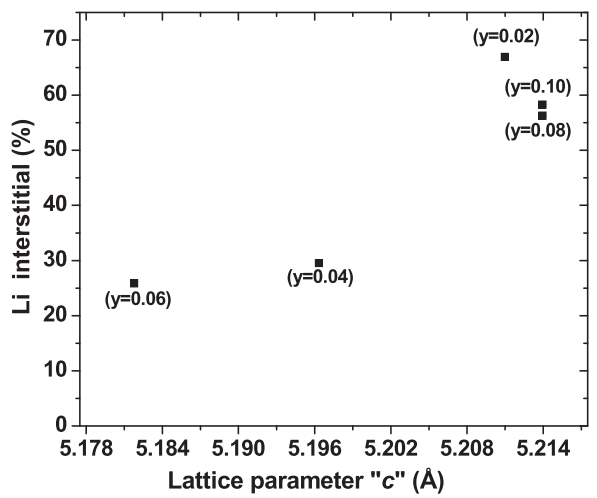

FIG. 6. Variation of Li interstitial defects extracted from peak deconvolution of Li 1s XPS spectra plotted with lattice parameter "*c*" for various concentrations of Li.

C. Magnetic measurements

The samples were consistently handled to avoid any possibility of magnetic contamination. The ferromagnetic (FM) hysteresis loops were measured at room temperature (RT ~ 300 K) and low temperature (LT ~ 50 K) of all samples. The undoped pure ZnO sample was fabricated and treated under the same condition as doped ZnO samples. The hysteresis curve of undoped ZnO sample before subtracting the effect of sample holder exhibits diamagnetic behavior both at RT and LT. The raw data (RT) of most of the compositions (before subtracting the background of sample holder from the data) and of the sample holder itself are shown in the upper left inset of Fig. 7(a). The background of the sample holder was subtracted from the raw data and from the resultant data the magnetization in terms of emu/g was calculated. The y = 0 composition also showed hysteresis after subtracting the sample holder back ground, however, the hysteresis curve was not fully saturated and diamagnetic features were still present as shown in Fig. 7(a). The hysteresis curve also shows remanant magnetization (M_r) and coercivity (H_c) as shown in the lower right inset in Fig. 7(a). As reported,[4,19,21] the existence of intrinsic defects in undoped ZnO can drastically affect the magnetic properties of nano ZnO systems as compared to bulk systems.

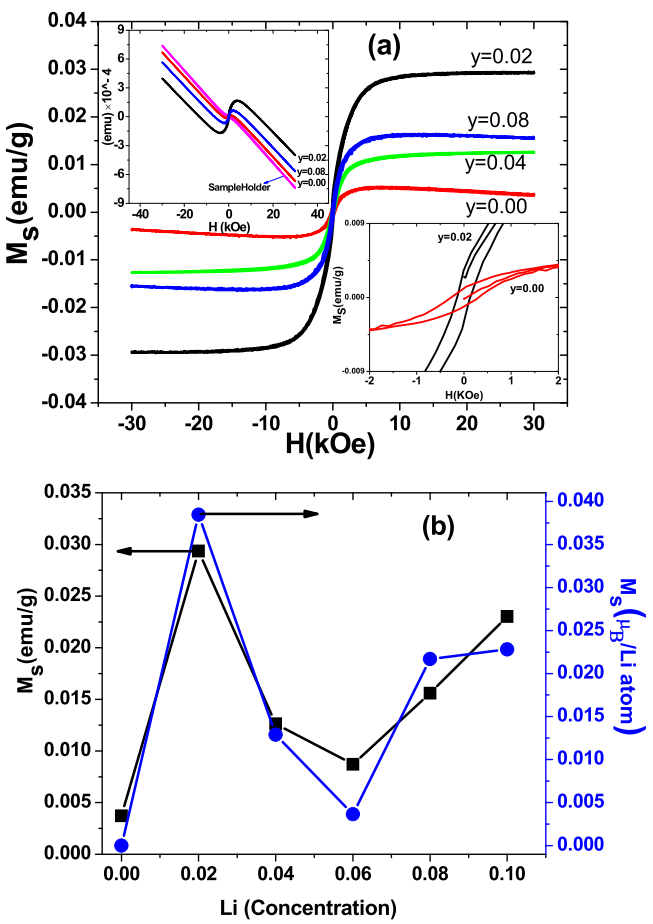

FIG. 7. (a) Hysteresis loop for some concentrations (y = 0, 0.02, 0.04, and 0.08) recorded at 300 K. In insets: upper left corner (y = 0.00) and lower right corner (y = 0.02) are shown in order to highlight the coercivity. (b) Room temperature magnetization for all concentrations is shown.

Fig. 7(a) shows the magnetic response for 2%, 4%, and 8% Li doped concentrations after subtracting the diamagnetic back ground of the sample holder and the clear hysteresis loops confirm ferromagnetic behavior of compositions. The insets in Fig. 7(a) demonstrate the values of remanence (M_r) and coercivity (H_c). The variations in measured values of M_s and moment μ_B/Li-atom as a function of Li concentration are plotted in Fig. 7(b). At 300 K, the value of 0.02936 emu/g is the maximum for the saturation magnetization for the 2% and a minimum value of 0.00872 emu/g value for the 6% Li doped ZnO sample as shown in Fig. 7(b). The moment varies in the range 0.0053-0.03846 (μ_B/Li) atom for doped ZnO samples at 300 K. Different groups have measured the magnetic moment for group 1 A elements, e.g., H, Li, Na, and K doped ZnO at 300 K. Khalid and Esquinazi[22] found large magnetization (~4.0 emu/g) for H implanted ZnO single crystal. In a ZnO nanowires system doped with the magnetic 4f element Nd, a high saturation magnetization of 4.5 emu/g was observed at room temperature.[23] The large value of the Nd doped system is, however, attributed to the interplay of the spin moments and the orbital derived moment of Nd. Chawla *et al.*[1,5] reported the saturation magnetization ~0.055 emu/g which was largest for 2% Li doped ZnO nanocrystalline powders. Saturation magnetization of 0.040 and 0.020 emu/g was measured for 2% and 10% Na doped ZnO nanorods,[1] while Li doped ZnO thin films yielded magnetization in the range 0.00–1.75 emu/cm^3 for varying Li concentrations i.e., $0.00 \leq y \leq 0.16$.[15] Ghosh *et al.*[24] measured saturation magnetization for $Zn_{1-x}K_xO$ nanowires for $0.00 \leq x \leq 0.08$, in the range of 0.008–0.038 emu/g. In a somewhat similar system to ours (Cu doped ZnO nanoparticles with 2% Cu), a magnetization of about 0.028 emu/g was measured at 300 K.[25] Our measured values, where the dopant Li carries no moment itself, thus appear to be comparable to the values reported for nanopowders or nanorods of similar composition, i.e., without a magnetic dopant.

Comparing the variation in M_s with Li concentration in Fig. 7(b) with the variation of Li interstitial and substitutional concentrations from Fig. 5(d), we note that the moment is large in the region where the Li interstitial concentration is large and vice versa. In the range where interstitial content is low, the system has a larger concentration of substitutional Li (Fig. 5(d)) suggesting that the moment is low when Li substitutes at a Zn site.

We notice an interesting correlation between the trend in coercivity and interstitial Li defects concentration. To illustrate this feature, we have shown in Fig. 8 the variation of the coercivity with the interstitial Li of the respective compositions. It is noticeable that the data separate into two parts, viz., the low coercivity data of 2%, 8%, and 10% with interstitial Li and the relatively higher coercivity data of 4% and 6%. However, what is interesting here is that the high coercivity compositions (4% and 6%) are also the ones that have lower Li_i concentrations and conversely, higher substitutional defects Li_{zn}. This trend is shown in the inset of Fig. 8. Defects are generally known to affect the coercivity[26] of ferromagnetic systems profoundly and it seems that in these nanoparticles larger concentration of Li substitutional defects enhances the coercivity.

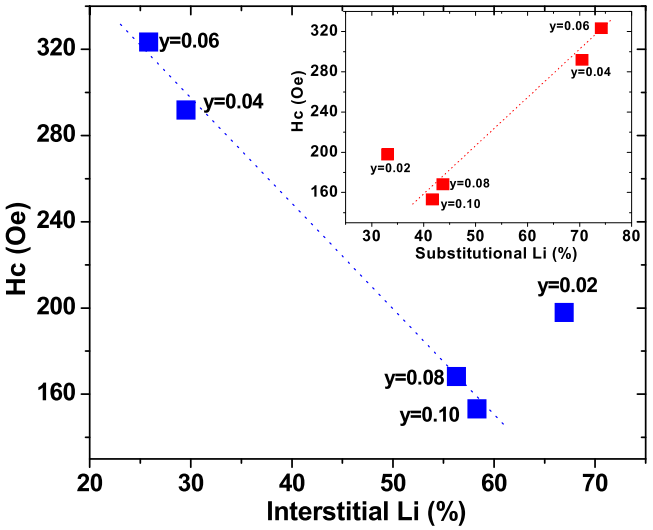

FIG. 8. Coercivities (H_c) versus the interstitial Li defect concentrations recorded at 300 K. Inset shows the coercivity versus substitutional Li defect concentrations.

The effects of irreversibility and coercivity were explored by measuring the low temperature magnetization as shown in Fig. 9. Here, we show the zero field cooled (ZFC) and field cooled (FC) magnetization for selected compositions to illustrate the trend. The field used in both cases was 500 Oe. First, we note that the moment shows very weak temperature dependence indicating that the critical temperature of the system is well above the highest temperature, viz., 300 K. As expected for a system with either spin freezing due to anisotropy effects or competing interactions, as in a spin glass, the two sets of data separate out at lower temperatures in all three compositions. Noticeably, the ZFC data do not decline at lower temperatures, as is usually the case for magnetic nanoparticles below the blocking temperature, but exhibit a very slight increase over the entire range of temperature 50–300 K. The field cooled data show the moment continuing to increase all the way down to 50 K. The absence of a peak in the ZFC moment suggests that the differences between the ZFC and

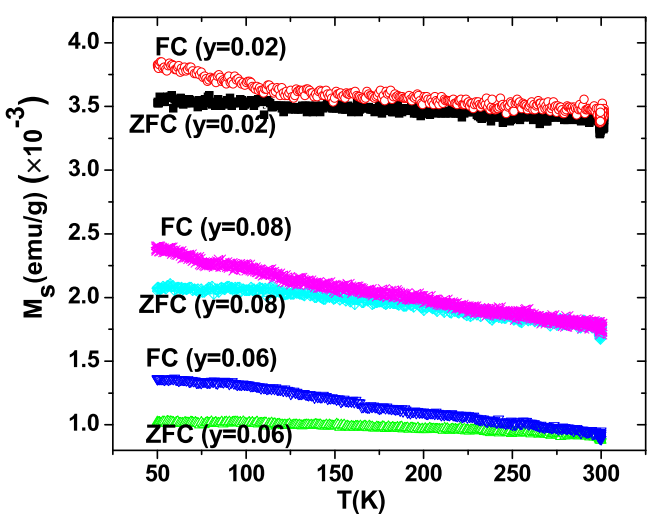

FIG. 9. FC and ZFC magnetization versus temperature for $y = 0.02$, 0.06, and 0.08 nanoparticles measured at 500 Oe.

FC data are not due to a general progressive freezing of the moments along some preferred directions or blocking due to competing interactions. The field cooled data, however, show that there must be some spins that are blocked even at room temperature and gradually align themselves with the field on cooling. Two other features are noticeable in these data. For the 6% sample, which has the highest coercivity, the separation between the FC and ZFC data starts out at the highest temperature of the three compositions (~300 K) and the extent of irreversibility (M_{FC}-M_{ZFC}) is also largest in the entire temperature range. As discussed above, the 2% and 8% compositions shown have low coercivity and larger moments and in this M(T) data, consistently exhibit lower extent of irreversibility. The strong irreversibility in the measured temperature range may be attributed, as is usual, to the presence of magnetically glassy phase. The system, we note, has inherent disordered where Li ions, that induce the magnetic behavior, are randomly distributed in ZnO host materials at interstitial and substitution sites. The interactions between these randomly distributed magnetic complexes result in a phase with glassy-like magnetic properties.[27]

III. CONCLUSION

The structural, electronic, and magnetic properties of Li doped ZnO nanoparticles reported here show various features that relate the development of ferromagnetism to the abundance of specific defects in these systems. Considering the variation of the moment with increasing Li content and correlating the changes with the Li interstitial and substitutional concentrations, an interesting correlation emerges. First, we note that the oxygen vacancy concentration to the limit of our resolution is constant over the various Li concentrations. Hence, any changes observed in the moment may not be attributed to the effects of oxygen vacancy concentration which in any case is expected to act as an n-type dopant, while the ferromagnetism of Li doped system should be of the hole or p-type. We have shown that the 2%, 8%, and 10% Li concentrations which have larger magnetic moments also exhibit larger Li interstitial concentrations. (A similar feature is observed in the case of zinc interstitial concentration but it is not stressed since the variations are somewhat small). This is the principal result of the current study. We note from comparison of Figs. 5(d) and 7(b) the marked similarity of the trends in their variation. For example, for the 4% and 6% concentrations that have low magnetic moments the interstitial Li also has low content while Li substitutional has a relatively high concentration. Thus, our results point towards the critical role of Li interstitials in stabilizing the ferromagnetism in ZnO nanoparticles. Hence, it is apparent that Li, which is in the substitutional state would be a monovalent ion and as such a hole dopant does not lead to enhanced moment, but does appear to do so in its interstitial state. We understand this trend as being indicative of the indirect role that Li plays in the development of the magnetic moment, viz., by stabilizing zinc vacancies. As mentioned above, each interstitial cation (e.g., Li) will most likely be accompanied by a cation vacancy which in this case would be a vacant zinc site. Hence, large concentration of interstitial lithium is an indicator of zinc vacancy which we recognize as the primary source of the moment. It may be noted that in the simulations of Yi *et al.*,[15] defect ferromagnetism in Li doped ZnO is stabilized by the formation of a complex that includes a zinc vacancy, Li interstitial and Li substitution. Zinc vacancies introduce magnetic moments as well as additional holes. We note that our XPS data show directly or indirectly the presence of all these three defects and correspond well with this picture. The observed high temperature ferromagnetism is possibly related to the coupling of these local moments by the high concentration of holes introduced by Li_{Zn} and V_{zn}. Our data, however, also show the limitations inherent in defect related ferromagnetism. As the concentration of the dopant (Li) increases beyond a certain limit, the trend towards interstitial Li begins to decrease and the substitutional Li begins to dominate with negative effects on the ferromagnetism. One of the primary challenges, thus, in developing materials with defect mediated ferromagnetism remains to stabilize such defects to higher dopant concentrations where the magnetic moments and critical temperatures are also larger.

ACKNOWLEDGMENTS

S. K. Hasanain and Saif-Ullah Awan acknowledge the financial support from the Higher Education Commission of Pakistan under "5000 Indigenous Ph.D fellowship program" and the project "Development and Study of Magnetic Nanostructures." We also acknowledge Dr. Everett E. Carpenter and Dr. Dmitry Pestove for providing the XPS and VSM facilities at Nanomaterial Core Characterization (NCC), Virginia Commonwealth University, Richmond USA.

[1]S. Chawla, K. Jayanthi, and R. K. Kotnala, J. Appl. Phys. **106**, 113923 (2009).
[2]S. A. Wolf, D. D. Awschalom, R. A. Buhrman, J. M. Daughton, S. von Molnar, M. L. Roukes, A. Y. Chtchelkanova, and D. M. Treger, Science **294**, 1488 (2001).
[3]M. H. F. Sluiter, Y. Kawazoe, P. Sharma, A. Inoue, A. R. Raju, C. Rout, and U. V. Waghmare, Phys. Rev. Lett. **94**, 187204 (2005).
[4]S. B. Zhang, S. H. Wei, and A. Zunger, Phys. Rev. B **63**, 075205 (2001).
[5]S. Chawla, K. Jayanthi, and R. K. Kotnala, Phys. Rev. B **79**, 125204 (2009).
[6]H. Peng, H. J. Xiang, S.-H. Wei, S.-S. Li, J.-B. Xia, and J. Li, Phys. Rev. Lett. **102**, 017201 (2009).
[7]B. Xiao, Z. Ye, Y. Zhang, Y. Zeng, L. Zhu, and B. Zhao, Appl. Surf. Sci. **253**, 895 (2006).
[8]J. G. Lu, Y. Z. Zhang, Z. Z. Ye, Y. J. Zeng, H. P. He, L. P. Zhu, J. Y. Huang, L. Wang, J. Yuan, B. H. Zhao, and X. H. Li, Appl. Phys. Lett. **89**, 112113 (2006).
[9]J. J. Lander, J. Phys. Chem. Solids **15**, 324 (1960).
[10]C. H. Park, S. B. Zhang, and S.-H. Wei, Phys. Rev. B **66**, 073202 (2002).
[11]M. G. Wardle, J. P. Goss, and P. R. Briddon, Phys. Rev. B **71**, 155205 (2005).
[12]E.-C. Leea and K. J. Chang, Physica B **376–377**, 707 (2006).
[13]Y. J. Zeng, Z. Z. Ye, J. G. Lu, W. Z. Xu, L. P. Zhu, and B. H. Zhao, Appl. Phys. Lett. **89**, 042106 (2006).
[14]Y.-H. Lin, M. Ying, M. Li, X. Wang, and C.-W. Nan, Appl. Phys. Lett. **90**, 222110 (2007).
[15]J. B. Yi, C. C. Lim, G. Z. Xing, H. M. Fan, L. H. Van, S. L. Huang, K. S. Yang, X. L. Huang, X. B. Qin, B. Y. Wang, T. Wu, L. Wang, H. T. Zhang, X. Y. Gao, T. Liu, A. T. S. Wee, Y. P. Feng, and J. Ding, Phys. Rev. Lett. **104**, 137201 (2010).
[16]M. Naeem, S. K. Hasanain, M. Kobayashi, Y. Ishida, A. Fujimori, S. Buzby, and S. I. Shah, Nanotechnology **17**, 2675 (2006).

[17]P. D. B. Vincent Crist, *Handbook of The Elements and Native Oxides* (XPS International, Inc., 1999), Vols. 1 and 2.
[18]U. Ilyas, R. S. Rawat, T. L. Tan, P. Lee, R. Chen, H. D. Sun, L. Fengji, and S. Zhang, J. Appl. Phys. **110**, 093522 (2011).
[19]M. Khalid, M. Ziese, A. Setzer, P. Esquinazi, M. Lorenz, H. Hochmuth, M. Grundmann, D. Spemann, T. Butz, G. Brauer, W. Anwand, G. Fischer, W. A. Adeagbo, W. Hergert, and A. Ernst, Phys. Rev. B **80**, 035331 (2009).
[20]R. K. Singhal, A. Samariya, S. Kumar, Y. T. Xing, U. P. Deshpande, T. Shripathi, S. N. Dolia, E. B. Saitovitch, Phys. Status Solidi A **207**, 2373 (2010).
[21]A. Janotti and C. G. Van de Walle, Phys. Rev. B **76**, 165202 (2007); S. Mal, S. Nori, C. Jin, J. Narayan, S. Nellutla, A. I. Smirnov, and J. T. Prater, J. Appl. Phys. **108**, 073510 (2010); G. Z. Xing, Y. H. Lu, Y. F. Tian, J. B. Yi, C. C. Lim, Y. F. Li, G. P. Li, D. D. Wang, B. Yao, J. Ding, Y. P. Feng, and T. Wu, AIP Adv. **1**, 022152 (2011).
[22]M. Khalid and P. Esquinazi, Phys. Rev. B **85**, 134424 (2012).
[23]D. Wang, Q. Chen, G. Xing, J. Yi, S. R. Bakaul, J. Ding, J. Wang, and T. Wu, Nano Lett. **12**, 3994 (2012).
[24]S. Ghosh, G. G. Khan, B. Das, and K. Mandal, J. Appl. Phys. **109**, 123927 (2011).
[25]R. Elilarassi and G. Chandrasekaran, J. Mater. Sci.: Mater Electron. **21**, 1168 (2010).
[26]S. Chattopadhyay, S. K. Neogi, A. Sarkar, M. D. Mukadam, S. M. Yusuf, A. Banerjee, and S. Bandyopadhyay, J. Magn. Magn. Mater. **323**, 363 (2011); W. B. Mi, H. L. Bai, W. B. Mi, H. L. Bai, and C. Q. Sun, J. Appl. Phys. **101**, 023904 (2007); Y. W. Heo, M. P. Ivill, K. Ip, D. P. Norton, S. J. Pearton, J. G. Kelly, R. Rairigh, A. F. Hebard, and T. Steiner, Appl. Phys. Lett. **84**, 2292 (2004).
[27]S. K. Mandal, T. K. Nath, A. K. Das, and D. Karmakar, J. Appl. Phys. **101**, 063913 (2007).